Hydrogen passivation of silicon surfaces: A classical molecular-dynamics study

U. Hansen and P. Vogl
Physik-Department and Walter Schottky Institut, Technische Universität München, Am Coulombwall, D-85748 Garching, Germany
(Received 27 October 1997; revised manuscript received 12 January 1998)

We present a computationally efficient classical many-body potential that is capable of predicting the energetics of bulk silicon, silicon surfaces, and the interaction of hydrogen with silicon. The potential includes well established models for one-component Si and H systems and incorporates a newly developed Si-H interaction. It is shown that the present model yields hydrogen diffusion barriers, hydrogen abstraction, and H_2 desorption reactions on silicon surfaces in excellent agreement with experiment and/or previous *ab initio* results. Detailed molecular-dynamics simulations are performed that elucidate the complex balance between adsorption and abstraction reactions during hydrogen passivation on Si(100) surfaces. We find a very high sticking coefficient of 0.6 for atomic hydrogen on clean Si(100)2×1 surfaces and provide a detailed qualitative and quantitative explanation for this prediction. Furthermore, we find that there are two efficient competing surface reactions of atomic hydrogen with monohydride Si surfaces. One is the Eley-Rideal abstraction of H_2 molecules, and the other one is adsorption. Additionally, adsorbed hydrogen on hydrogenated Si surfaces acts as a reservoir that can lead to complete passivation of Si surfaces despite the efficient creation of voids in the hydrogen layer by the abstraction. [S0163-1829(98)00620-1]

I. INTRODUCTION

The extremely complex microscopic processes that take place on silicon surfaces during chemical vapor deposition (CVD), passivation, or wet chemical cleaning are still puzzling and surprisingly poorly understood,[1] in spite of the extraordinary technological relevance of these processes.[2,3] While many intriguing and sophisticated experiments have shed light on specific aspects of adsorption or desorption processes in recent years,[4–7] the microscopic processes that play a role in the hydrogen passivation or other hydrogen reactions at silicon surfaces are still under debate.[8–11]

From a theoretical side, most surface deposition processes occur on time scales and sample sizes that are beyond the scope of first-principle approaches,[1] even though they constitute an indispensable tool for reliable predictions of ground-state properties.[12–14] It is the immediate goal of the present work to develop a carefully designed and computationally efficient classical many-body potential that allows one to study the reaction dynamics of atomic hydrogen with silicon surfaces. While the precision and reliability of classical potentials is clearly inferior to quantum-mechanical first-principles approaches,[15] it still useful to have at hand an approximate but quick scheme to identify and analyze Si-H reaction processes. In situations that involve intrinsically dynamic nonequilibrium processes, classical molecular-dynamics schemes often constitute the only framework that allows a realistic prediction of dominant reaction paths. In addition, we will show that the present classical dynamics study provides a vivid and physically transparent insight into the transient dynamics of hydrogen passivation.

For the passivation of silicon surfaces such as the technologically most relevant Si(100) surface, one uses atomic hydrogen H or deuterium D, since the sticking coefficient of molecular hydrogen on Si surfaces is known to be extremely low.[6,16] For a long time, the only relevant reaction in the passivation process was believed to be the direct adsorption of H onto the Si dangling bonds (denoted by $*-$Si),[4]

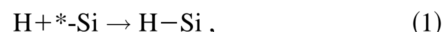

$$\mathrm{H}+{*}\text{-Si} \rightarrow \mathrm{H}-\mathrm{Si}\,, \tag{1}$$

even though, to the best of our knowledge, the rate of this reaction has never been established for Si(100)2×1 surfaces. In addition, one has recently found very efficient desorption processes that compete with the former adsorption reaction, namely[4,5,17]

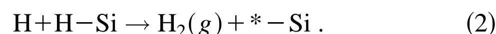

$$\mathrm{H}+\mathrm{H}-\mathrm{Si} \rightarrow \mathrm{H}_2(g)+{*}-\mathrm{Si}\,. \tag{2}$$

The use of different isotopes made it possible to unambiguously discriminate between molecules that form during the reaction with the surface and within the gas phase, respectively. These experiments[4,5,17] indicated that the abstraction reactions are exothermic processes with a relatively large energy gain of approximately 1 eV per H_2 molecule and involve an Eley-Rideal (ER) abstraction mechanism. Indeed, the data showed reaction (2) to occur with a high probability of 0.3 ± 0.2 and to be nearly independent of the incident kinetic energy, as is typical for nonactivated processes.

These data have opened up the question of why passivation with atomic hydrogen works at all or, phrased differently, why the above exothermic desorption processes do not limit the achievable maximal hydrogen coverage and thus the quality of passivation. To be sure, STM images[18] and LEED data[19] have revealed perfectly ordered (2×1) monohydride phases at 600 K, with a hydrogen coverage very close to 1 monolayer.

In this paper, we present detailed molecular dynamics simulations to elucidate the complex balance between adsorption and desorption during hydrogen passivation on Si(100) surfaces. We have calculated the sticking coefficient for reaction (1), the probability of H abstraction such as reaction (2), as well as the adsorption of additional H on the hydrogenated surface that will be shown in this work to play a dominant role in maintaining complete H-coverage.

 © 1998 The American Physical Society

This paper is arranged as follows. In Sec. II, we present and explain the presently developed Si-H potential model. Section III provides a critical assessment of this potential. We have computed a wide range of surface and bulk properties with it and compare the results with experimental and previous theoretical findings. Section IV discusses computational details such as supercell sizes and statistics. Sections V and VI present the central predictions of this paper. Section V deals with the sticking coefficient of atomic H on Si surfaces, and Sec. VI provides a detailed account of surface reactions relevant for H passivation. The paper ends with a summary (Sec. VII).

II. THE Si-H INTERATOMIC POTENTIAL

In this paper, we wish to develop a classical many-body potential for systems containing silicon and hydrogen. Previously developed classical empirical interatomic potentials for the Si-H interaction[20–23] have focused on bulk and molecular rather than surface related properties. In this section, we generalize these models to properly account for Si-H interactions at Si surfaces, yet to reproduce the known molecular properties (such as bond lengths, vibrational frequencies, and binding energies) of silicon hydride molecules.[22,23] The functional form of this model potential is based on Ref. 23 and contains four additional Si-H parameters. The Si-Si interaction is taken to be the Tersoff-3 potential[24] and we have employed the Brenner model[25] for the H-H part. The latter two models have been critically assessed and tested extensively in the literature.[26,27] We represent the total potential energy of a sample containing Si and H atoms in the form of three-body terms that are written as a sum of *ordered* atom pairs,

$$V=\sum_{i>j}[\phi(i,j)+\phi(j,i)]f_c(r_{ij}),$$

$$\phi(i,j)=a_1B_1[N(i,j)]\exp(-\lambda_1 r_{ij}) - a_2B_2[N(i,j)]\exp(-\lambda_2 r_{ij}) \times\left\{1+\left(\sum_{k\neq(ij)}\xi(i,j,k)\right)^{\eta}\right\}^{-\delta}. \quad (3)$$

Here, r_{ij} denotes the distance between particles i and j. The range of all interactions is constrained by a smooth cutoff function $f_c(r_{ij})=f_c(r_{ji})$ that depends on the type and distance between the atoms i,j. It is set equal to 1 for $r_{ij}<R-D$ and to 0 for $r_{ij}>R+D$, and

$$f_c(r_{ij})=\frac{1}{2}-\frac{9}{16}\sin\left(\pi\frac{r_{ij}-R}{2D}\right)-\frac{1}{16}\sin\left(3\pi\frac{r_{ij}-R}{2D}\right) \quad (4)$$

for the range $R-D<r_{ij}<R+D$. The parameters a_1, a_2, λ_1, λ_2, η, δ, R, and D in the equations above are symmetric with respect to the particles i and j and are summarized in Table I. In order to avoid index cluttering, we have omitted the indices i,j wherever it is unambiguously possible to do so. The quantity $N(i,j)$ is defined as

TABLE I. Parameters entering the potential term $\phi(i,j)$ and the cutoff function $f_c(r_{ij})$ as a function of the atom pair (i,j), where i and j can be either silicon or hydrogen. The units of each parameter are given in parentheses; η and δ are dimensionless.

Parameter	(Si,Si)	(Si,H)	(H,H)
a_1 (eV)	1830.8	323.54	80.07
a_2 (eV)	471.18	84.18	31.38
λ_1 (Å)	2.4799	2.9595	42.075
λ_2 (Å)	1.7322	1.6158	1.7956
η	0.78734	1.00	1.00
δ	0.635	0.80469	0.80469
$R^{(e)}$ (Å)	2.35	1.475	0.74
R (Å)	2.85	2.25	1.40
D (Å)	0.15	0.15	0.30

$$N(i,j)=\begin{cases}\sum_{k\neq i} f_c(r_{ik}) & \text{for } i=\text{Si}, j=H,\\ \sum_{k\neq j} f_c(r_{jk}) & \text{for } i=H, j=\text{Si}.\end{cases} \quad (5)$$

The sum over k runs over all atoms in the sample. The function $N(i,j)$ represents the effective number of nearest neighbors of the Si atom in the pair (i,j). The real valued functions $B_1(N)$ and $B_2(N)$ in Eq. (3) characterize the bond strength between particle pairs i and j. If atom type i equals atom type j, we set $B_1(N)=B_2(N)=1$ irrespective of the value of N. For unlike atom pairs (i,j), the functions B_1 and B_2 are given in Table II for integer argument values N, and have been spline interpolated for noninteger values. Equation (3) contains, in addition, a three-body term that is always greater or equal to zero and weakens the attractive potential part, and is given by

$$\xi(i,j,k)=f_c(r_{ik})\left[c(i,j,k)+d(i,j,k)\times\left\{\Theta[M(i,j,k)]-\frac{\mathbf{r}_{ij}\cdot\mathbf{r}_{ik}}{r_{ij}r_{ik}}\right\}^2\right] \times\exp\{\alpha(i,j,k)[(r_{ij}-R_{ij}^{(e)})-(r_{ik}-R_{ik}^{(e)})]^{\beta(i,j,k)}\}. \quad (6)$$

For a two-particle system, the expression $\xi(i,j,k)$ is set equal to zero. The distance parameter $R_{ij}^{(e)}$ is given in Table I. The three-body parameters $\alpha(i,j,k)$, $\beta(i,j,k)$, $c(i,j,k)$, and $d(i,j,k)$, depend on the *ordered* triplets $\{i,j,k\}$ and are summarized in Table III. The real valued function $\Theta[M(i,j,k)]$ determines the energetically optimal angular

TABLE II. Values for the functions $B_1(N)$, $B_2(N)$, and $\Theta(M)$ that enter the Si-H potential for integer arguments N and M.

N	$B_1(N)$	$B_2(N)$	$\Theta(M)$
1	1.005	0.930	−0.040
2	1.109	1.035	−0.040
3	0.953	0.934	−0.276
⩾4	1.000	1.000	−0.470

TABLE III. Dimensionless parameters for the many-body term $\xi(i,j,k)$ of the Si-H potential as a function of the ordered triplets $\{i,j,k\}$.

	{Si,Si,Si}	{Si,Si,H}, {Si,H,H}, {Si,H,Si}	{H,Si,Si}	{H,H,H}, {H,H,Si}	{H,Si,H}
α	5.1975	4.00	0.00	3.00	2.2
β	3	3	1	1	1
c	0.00	0.0216	0.70	4.00	1.23
d	0.160	0.27	1.00	0.00	0.0
Θ	−0.059826		−1.00	0.00	0.0

distribution of the atoms $\{i,j,k\}$. $\Theta(M)$ is taken to be constant for the ordered triplets $\{i,j,k\}$ $=\{$Si,Si,Si$\}$,$\{$H,Si,Si$\}$,$\{$H,Si,H$\}$,$\{$H,H,Si$\}$,$\{$H,H,H$\}$ irrespective of the value of M. The corresponding constants are given in Table III. For the triplets $\{i,j,k\}$ $=\{$Si,Si,H$\}$,$\{$Si,H,Si$\}$, and $\{$Si,H,H$\}$, on the other hand, the function $\Theta(M)$ is given for integer argument values M in Table II and is spline interpolated for noninteger values of M. The quantity $M(i,j,k)$ itself is defined as $M(i,j,k)$ $=\Sigma_{n\neq i}f_c(r_{in})$, where n runs over all atoms.

The two Si-H cutoff parameters R and D in Table I differ from those of Ref. 23 and have been fitted to properly account for the total energies of Si containing interstitial hydrogen at the H and T site (see Sec. III B). In addition, we have chosen the many-body Si-H parameters α and c for the triplet {H,Si,H} to reproduce first-principles results for the H_2 desorption barrier height (Sec. III D) and to ensure the existence of an exothermic path in the Si-H potential energy surface of the Eley-Rideal abstraction (see Sec. III E).

Without the three-body term $\xi(i,j,k)$, the potential would only yield closed packed structures. Thus, this term is important for stabilizing structures such as the diamond structure of bulk Si. To further illustrate the expression Eq. (6), let us consider the equilibrium geometry of a SiH_2 molecule. In this case, only the triplet $\{$Si,H,H$\}$ contributes to $\xi(i,j,k)$. This yields $M=2.0$ and, correspondingly, $\Theta[2.0]=-0.040$ (see Table II). Thus, the term $[\Theta[M]-\mathbf{r}_{ij}\cdot\mathbf{r}_{ik}/(r_{ij}r_{ik})]^2$ in Eq. (6) becomes minimal for an angle of 92.3° in accordance with experiment.[28]

In the subsequent sections, we will apply this Si-H potential also to Si-D systems without modification since the tiny differences due to nuclear spin effects are negligible.

III. ASSESSMENT OF THE POTENTIAL

In this section, we show that the empirical potential developed in this paper yields results for H diffusion and desorption that are in excellent agreement with *ab initio* results and with experiment. Earlier models[20–23] involving Si and H focused on Si-H molecular energies and have not been optimized for accurately capturing H-related diffusion barriers. As a consequence, H diffusion barriers such as discussed below were typically off by a factor of 2 and some exothermic reactions such as the abstraction of already absorbed H were endothermic.

TABLE IV. Calculated total energies of bulk Si with a hydrogen atom in various interstitial positions. All energies are given in eV and relative to the total energy of Si with an H atom at the tetrahedral site $(a/2)(111)$. The other interstitial sites are labeled by H (hexagonal), C (C site), and bc (bond centered), respectively (Ref. 33). All coordinates refer to the conventional unit cell of lattice constant a.

Interstitial position		Energy (eV) Present theory	Previous theories
H	$\frac{5}{8}a(111)$	0.59	0.60 [a]
C	$\frac{1}{4}a(122)$	3.7	3.1, [b]
bc	$\frac{1}{8}a(331)$	−1.23	−0.88, [b] −1.2 [c]

[a]Reference 33.
[b]Reference 34.
[c]Reference 32.

A. Si surfaces

Since the Si-Si interaction in our model potential is identical to the Tersoff-3 potential,[24] it reproduces the same surface properties that have been reviewed in Refs. 24,26 and 15. For a free Si(100) surface, the energy gain associated with a Si(100)2×1 reconstruction is found to be −1.6 eV per dimer, in good agreement with *ab initio* calculations that give values in the range of −1.5 to −1.8 eV.[29–31] As is well known, the short-range nature of the Tersoff-3 potential fails to capture the small energy difference of approximately −0.15 eV between the symmetric and asymmetric buckled dimers[30,31] and always yields a symmetric dimer ground state. Fortunately, our studies reveal that the buckling is unlikely to be of relevance for the adsorption and desorption processes of *atomic* hydrogen on clean or passivated surfaces, as will be discussed in Sec. VI.

B. H-interstitial diffusion barriers

We have calculated the total energy of bulk silicon containing a single hydrogen atom in various interstitial positions. We have taken a large Si supercell (see Sec. IV for details) with an H on the tetrahedral interstitial site as the reference system that sets the zero of energy. The energies of several other interstitial configurations are summarized in Table IV and can be seen to agree very well with first-principles local-density-functional (LDA) calculations[32] and *ab initio* Hartree-Fock-type calculations.[33,34] The diffusion barrier between the tetragonal and hexagonal site is particularly well reproduced by our model. For the bond centered position, all calculations fully included the relaxation of Si atoms. For the latter position, we find H to cause an elongation of the Si-Si bond by 30.4%, in excellent agreement with the Hartree-Fock value of 34%.[34] We note that the previous model of Refs. 22 and 23 yielded no energy difference between the tetragonal and hexagonal sites.

C. H adatom diffusion barriers

Hydrogen adatom diffusion barriers on Si surfaces are crucial in understanding hydrogen molecule desorption,[35] since the desorption process is believed to be initiated by adatom diffusion.[36,37] We have calculated the potential en-

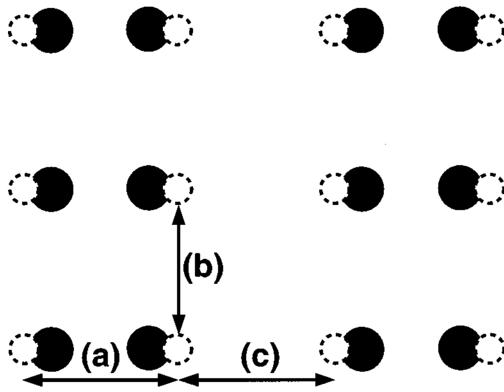

FIG. 1. Diffusion paths for atomic hydrogen on the Si(100)2×1 surface. The large black circles depict two parallel rows of dimers of the topmost Si layer. The small dotted circles show adsorption sites for atomic hydrogen, i.e., the dangling bond sites. Atomic hydrogen adsorbed at one of these positions can diffuse to a neighboring dangling bond site via intradimer diffusion (a), intrarow diffusion (b), or inter-row diffusion path (c).

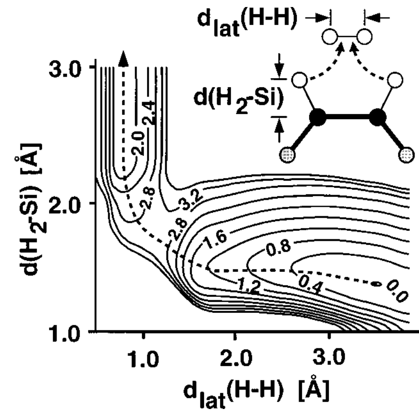

FIG. 2. Calculated potential energy surface for the symmetric recombinative H_2 desorption from a Si(100)2×1:H surface. In the inset, a schematic plot of the reaction geometry is depicted. The dashed line corresponds to the lowest energy reaction path from the surface to the gas phase. The contour plot shows the potential energy as a function of d_{lat}(H-H), i.e., the lateral distance between the H atoms, and the distance between the H_2 molecule and the surface, denoted by $d(H_2\text{-Si})$. The monohydride configuration is taken as zero of energy and the spacing of the contour lines is 0.4 eV.

ergy surface for hydrogen adatom diffusion, following the general procedure of Refs. 38 and 36. The H adatom is placed at various lateral positions within the Si(100)2×1 surface unit cell, and for each position the total energy is minimized with respect to the distance of the adatom from the surface. We have performed total energy minimizations both with fully optimized Si positions in the supercell as well as with frozen Si atoms. In accord with the first-principles LDA calculations of Ref. 36, we find the dangling bond position of H to be the most stable one (marked by dotted circles in Fig. 1). The local minima of the total energy indicate three major directions for H-adatom diffusion that are also plotted schematically in Fig. 1, namely the intradimer, intrarow, and interrow diffusion trajectories.[36] The energy maxima along each of these saddle lines define the diffusion barriers. They are summarized in Table V and compared to first-principles results[36,13,37] for unrelaxed and fully relaxed Si atom coordinates. The numerical details, such as supercell size, that were employed in our calculations are discussed in Sec. IV. As one can see from Table V, the various *ab initio* calculations differ appreciably from one another. However, all methods, including the present one, agree in that the highest barrier occurs for the inter-row diffusion and the lowest for the relaxed interdimer path. The present results lie within the range of the barrier heights predicted by the parameter-free methods. We find the Si lattice relaxation to be largest in the case of intradimer H diffusion where the dimer bond gets elongated by 37% from 2.37 Å to 3.23 Å.

TABLE V. H-adatom diffusion barriers on Si(100)2×1 surfaces, as calculated with the present model potential and previously within the local density approximation (LDA), the generalized gradient approximation (GGA), and the configuration interaction (CI). The diffusion paths are labeled according to Fig. 1. All barrier heights are in eV.

	Diffusion path	LDA [a]	GGA [b]	CI [c]	This work
relaxed	intradimer	1.2	1.9		1.1
	intrarow	1.3	2.4		1.8
	inter-row	2.2	3.1		2.4
unrelaxed	intradimer	2.5		1.1	2.6
	intrarow	2.0		2.0	2.3
	inter-row	2.7		2.9	3.2

[a]Reference 36.
[b]Reference 13.
[c]Reference 37.

As we have pointed out in Sec. III A, our calculations assume a symmetric dimer ground state, whereas the first-principles results are based on buckled surfaces. Nevertheless, we believe that the comparison between the two approaches is well justified for the following reasons. First, the effect of lattice relaxation of the dimer atoms during the diffusion process is much larger than the effect of buckling. Second, the diffusion barriers are much higher than the 0.15 eV gain in energy due to buckling. Third, the initial and final configuration in the diffusion process corresponds to a dimer where one bond is saturated with hydrogen. In this configuration, the dimer has been found to be already nearly symmetric (Ref. 45).

D. Recombinative hydrogen desorption

We have determined the potential energy surface for recombinative desorption[35,6] of H_2 from the Si(100)2×1:H monohydride phase, assuming the desorbing H_2 atoms to remain parallel to the surface. A schematic plot of this desorption mechanism is shown in the inset of Fig. 2. This figure depicts the total energy of the system as a function of the lateral H-H separation and the vertical distance between the H_2 molecule and the (frozen) Si surface. The neglect of lattice relaxation corresponds to a sudden desorption event[14] where the light H_2 molecule leaves the surface faster than the Si atoms can relax. If the perfect monohydride phase is taken as the zero of energy, we find the desorption barrier for H_2 to amount to 2.9 eV per molecule, in excellent agreement with first-principles generalized-gradient-corrected LDA

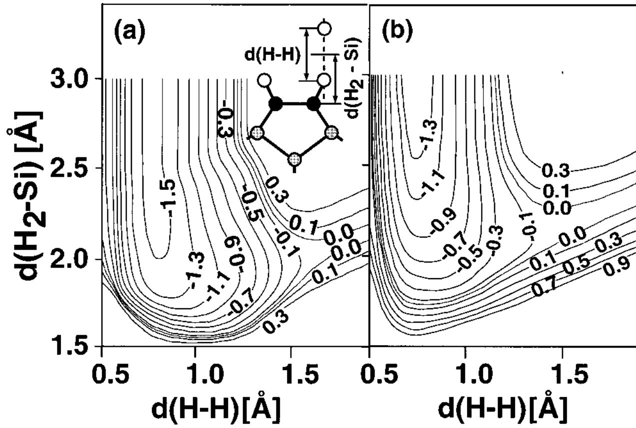

FIG. 3. Calculated potential energy surface for H_2 abstraction, as predicted by the present model (a) and by previous first-principles calculations (Ref. 39) (b). In both calculations the motion of the H atoms is constrained onto the dashed line as depicted in the inset of (a). The contour plots show the potential energy for this reaction as a function of the H-H separation d(H-H) and the distance between the H_2 molecule and the surface $d(H_2\text{-Si})$. The zero of energy is taken to be the monohydride phase. The spacing between the contour lines is 0.2 eV except between 0 and 0.1 eV.

calculations[14] that give 3.0 eV. Experimentally, this barrier height has been found to lie in the range between 2.0 and 2.9 eV (see Ref. 6 and references therein).

E. Eley-Rideal hydrogen abstraction

Next, we consider the removal of a chemisorbed H from the monohydride Si(100) 2×1:H surface by an additional H atom that approaches the surface, i.e., the Eley-Rideal H_2 abstraction reaction.[4,5,17] Figures 3(a) and 3(b) compare the total energy of a hydrogenated Si slab with an additional H atom that approaches the surface, as calculated by the present model and by a first-principles approach[39] that is based on the generalized-gradient-corrected LDA (GGA). These energy surfaces depict the calculated total energy as a function of two reaction coordinates that are indicated schematically in the inset of Fig. 3(a). The first one is the distance between the approaching and the adsorbed H atom and is denoted by d(H-H). The second coordinate is the distance between the center of mass of these two H atoms and the topmost Si layer and is labeled by $d(H_2\text{-Si})$.

In accordance with the GGA calculations[39] as well as in agreement with recent experiments,[4,5] the present calculations predict the H_2 abstraction [reaction (2)] to be exothermic. The agreement between the results in Figs. 3(a) and 3(b) is seen to be excellent. The energy gain per H_2 molecule in the exothermic abstraction amounts to -1.5 eV and -1.3 eV, respectively, in the two approaches. It originates in the difference between the binding energy of an H_2 molecule (-4.7 eV) and the binding energy of a single H atom attached to a dimer (-3.2 eV).

IV. COMPUTATIONAL DETAILS

For the bulk properties of Si with H, we have used three-dimensional supercells containing 216 Si atoms for unrelaxed as well as relaxed lattices. We have estimated the errors in total energies due to the finite size of the supercell to lie well below 0.05 eV. The forces $\mathbf{F}$ per atom have been minimized until $|\mathbf{F}|<10^{-4}$ eV/Å was reached for all atoms. In the total energy studies of surface related properties, we have employed finite slabs with periodic boundary conditions for the lateral cells. These supercells consisted of eight atomic layers and 144 Si atoms in total, which guaranteed the same level of convergence.

The dynamical simulations (see Secs. V and VI) called for larger lateral supercells containing 616 Si atoms, arranged in 11 atomic layers and 56 Si atoms per layer. The bottom two layers were fixed at their equilibrium positions, while all other atoms were allowed to move freely in response to the time-dependent potential. The equations of motion were integrated using a fourth order Runge Kutta algorithm, with time steps in the range 0.1–0.25 fs in order to ensure total energy conservation throughout the simulation.

The temperature of the substrate has been set by the following well established procedure:[40] Initially, random velocities are assigned to the atoms. Subsequently, the system is iteratively equilibrated for a period of several ps and the moduli of the velocities are rescaled until the average kinetic energy per unit cell corresponds to the desired sample temperature.

V. PREDICTIONS: STICKING COEFFICIENT OF ATOMIC HYDROGEN AND DEUTERIUM ON Si(100)2×1

The efficiency of H passivation of Si surfaces depends crucially on the sticking coefficient S of atomic hydrogen that is unknown for Si(100)2×1 surfaces. Experimental data for (111) surfaces indicate S to lie in the range between 0.5 and 1.[41] Since the present empirical model potential reproduces the energetics of the H-Si interactions faithfully, we have employed it to analyze the dynamics of atomic H adsorption as a function of incident kinetic energy. In addition, we have also analyzed the same process with atomic deuterium. In the latter case, we have taken the Si-D potential to be identical to the Si-H interaction potential so that D differs from H only through its larger mass.

We have performed extensive simulations for Si(100)2 ×1 surfaces at temperatures of 500 K, where H_2 desorption is still negligible. This condition corresponds to a set of experiments performed in Ref. 4. In our calculations, the incident H or D atom has been positioned outside the interaction range of the surface. Since atomic H is typically produced by dissociating H_2 molecules at a hot tungsten filament of ≈ 2000 K,[4,17] the initial velocities have been chosen to correspond to a kinetic energy of 0.1−0.3 eV. In addition, we have assumed vertical incidence of the H (or D) atom and chose its lateral position randomly relative to the substrate surface unit cell. Runs with nonzero incident angles up to 30° did not affect the results noticeably. The trajectory of each atom was monitored for a period of 200 fs, and 500 trajectories were analyzed for each incident energy. The time interval of 200 fs is sufficient to observe well-defined reflection or chemisorption processes. The size of the supercell and particularly the number of atomic layers (see Sec. IV) has been chosen large enough in the present simulations to guarantee that the periodic boundary conditions do not lead

TABLE VI. Calculated sticking probability of atomic hydrogen and deuterium on the Si(100)2×1 surface as a function of the incident kinetic energy of the hydrogen isotope. The surface temperature has been set to 500 K.

Energy (eV)	H	D
0.1	0.71	0.65
0.2	0.59	0.55
0.3	0.52	0.40

to artificial energy reflections within the simulation time.

First, we summarize the numerical results for S. These values were determined from the number of adsorption events, divided by the total number of computed trajectories. Table VI shows the results for incident kinetic energies in the range from 0.1 to 0.3 eV. Importantly, we find the adsorption probability for atomic H to be very high, in qualitative accord with experimental findings for the (111) surface and with the known efficiency of H passivation. The sticking coefficient of H and D decreases with increasing incident energy and is found to be slightly lower for D than for H. While the results in Table VI have been obtained with symmetric dimers, we do not expect them to change significantly for asymmetric charge distributions associated with buckled dimers as we find S not to change significantly when the dangling bond sites are occupied (see discussion in Sec. VI).

In order to gain insight into the mechanisms that lead to these high values of S, it is useful to analyze representative trajectories of impinging H atoms. Figures 4(a) and 4(b) show two distinct H trajectories that are projected onto the plane spanned by the (011) and (100) directions. For the sake of clarity, we only show the equilibrium positions of the substrate silicon atoms in these figures, even though their motion has been fully taken into account in the simulation and will be shown to be highly relevant for the chemisorption. Figure 4(a) shows an H trajectory for a period of 400 fs that leads to absorption of the H at one dangling bond site. By contrast, Fig. 4(b) shows a typical reflection process that occurs within the depicted period of 250 fs. The relevant portions of the two trajectories within the interaction range of the surface are much shorter and of the order of 200 and 30 fs for Figs. 4(a) and 4(b), respectively. The discriminating factor in these trajectories is the different initial position of the incoming H atom.

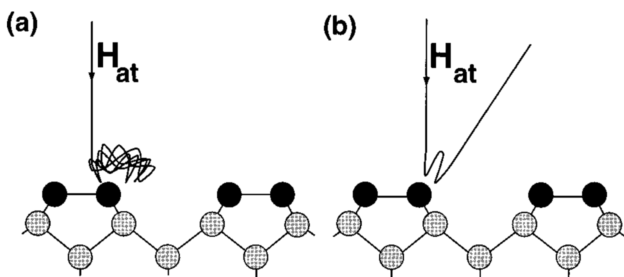

FIG. 4. Projection of the three-dimensional trajectories of hydrogen atoms impinging on the Si surface onto the (100) and the (011) plane. The black circles show the topmost Si atoms, the gray circles depict those of subsurface layers: (a) Typical direct adsorption event. This trajectory is shown for a period of 400 fs. (b) Typical direct reflection event for 250 fs. In both cases, the incident kinetic H energies are 0.1 eV. For the sake of clarity, the motions of the Si atoms are not shown.

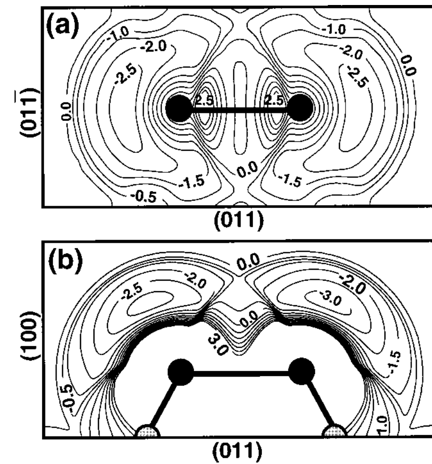

FIG. 5. (a) Snapshot of the potential energy surface for an H atom 1.1 Å above the topmost Si layer . The area shown corresponds to four surface unit cells. (b) Snapshot of the potential energy surface for an H atom moving in the (100) and (011) plane containing the dimer bond. In both cases, the black circles show the dimer atoms, and the gray circles the Si atoms of the second layer. The zero of energy is the clean surface and the spacing of the contour lines is 0.5 eV. In the highly repulsive region of (b), only values smaller than 3.0 eV are plotted.

There are three mechanisms that contribute to the high sticking probability of atomic H. First, the potential felt by the impinging H atom is strongly attractive on almost the entire surface. Second, the pronounced corrugation of this potential prolongs the interaction time and enhances energy dissipation in this way. The third factor is the efficient momentum and energy transfer to the Si lattice.

The first factor that contributes to S can be deduced from the potential surface that is felt by the incoming H atom. In Fig. 5(a), a snapshot of this potential surface is plotted at an altitude of 1.1 Å above the topmost Si layer. The potential is seen to be markedly attractive over the *whole* depicted area of four unit cells. Its shape is roughly that of attractive funnels centered around the dangling-bond positions; only close to the dimer bond, there are small repulsive protuberances.

The second effect of corrugation is illustrated in Fig. 5(b). This figure depicts the potential energy surface for an H atom moving in the (100) and (011) plane containing the dimer bond. The H potential is very steep vertically but consists of a long attractive valley perpendicular to the dangling bond. This valley provides a guiding channel for the impinging H that diminishes the probability of immediate reflection and increases the interaction time with the surface. We note that a similar effect is known to be responsible for the high adsorption rate of atomic H on Cu surfaces.[42]

To study the third factor of energy transfer to the substrate that eventually leads to adsorption, we have analyzed the time evolution of the incoming H atom's energy. Figure 6 shows the potential energy and total energy of the H atom as a function of time for two types of situations. In the first case, we keep the Si lattice rigidly fixed at the atoms' equilibrium positions; in the other case, the calculations take into account the motion of the Si atoms. In both cases, the H

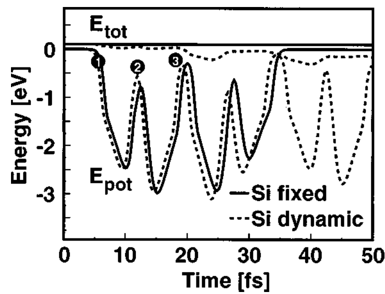

FIG. 6. Potential and total energy of an H atom approaching the Si surface as a function of time. Full line, rigid Si lattice rigid. H leaves the surface after 35 fs. Dashed line, dynamics of the Si atoms taken into account. H systematically loses energy and remains captured. The numbers mark characteristic points on the H trajectories.

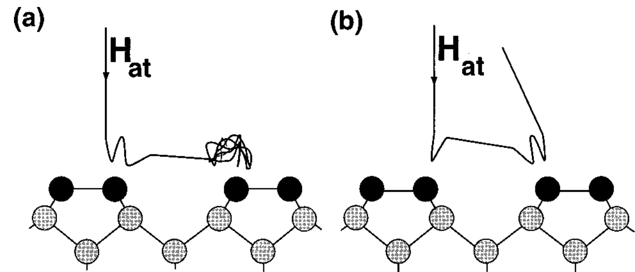

FIG. 7. Projection of the three-dimensional trajectories of hydrogen atoms approaching the Si surface onto the (100) and the (011) plane. The black and gray circles show the topmost and subsurface layer Si atoms, respectively. (a) Typical surface-mediated adsorption event. (b) Typical surface-mediated reflection event. In both cases, the incident kinetic H energies are 0.1 eV. For the sake of clarity, the motions of the Si atoms are not shown.

atom enters the attractive surface potential after approximately 5 fs (marked by 1) and penetrates the strongly attractive dangling bond funnel. At roughly 12 fs (marked by 2) it has reached the repulsive part of the potential behind the attractive dangling bond region. At this point, its potential becomes maximal and, correspondingly, its kinetic energy becomes minimal. Subsequently, the particle changes direction and moves outwards again until it reaches its outer turning point (marked by 3).

In the case of a rigid Si lattice, the total energy of the H atom is obviously conserved. Nevertheless, the long and deep valley formed by the dangling bond potential causes the H atom to oscillate typically once or twice inwards and outwards before becoming reflected into the gas phase after approximately 35 fs in Fig. 6. By contrast, with the motion of Si atoms taken into account, the H atom systematically loses energy to the lattice while being accelerated towards the Si atom. In spite of the small difference in the trajectory during the first 20 fs, the continuous energy loss of the order of 0.1 eV per oscillation cycle (such as positions 1 to 3 in Fig. 6) makes it increasingly difficult with time for the H atom to escape. Indeed, we find that reflections back into the gas phase can only occur within the first 20 fs. The energy loss is a consequence of the strongly attractive Si-H interaction. The temperature-induced lattice vibrations occur on a fairly long time scale of typically 70 fs. Therefore, they do not significantly alter the energy exchange mechanisms and, in turn, the value of S. Finally, we note that its decrease with increasing kinetic energy of the H atom is simply due to the larger amount of energy that has to be dissipated.

The trajectories depicted in Fig. 4 account for about 50% of S. Our studies have revealed another type of capture or reflection process that may be termed surface mediated. In this case, the hydrogen atom hits the surface and traverses to a neighboring dangling bond region where it gets either chemisorbed or reflected. Typical processes of this type are depicted in Figs. 7(a) and 7(b). There is a preferential deflection towards the neighboring dimer row because of the shape of the potential energy surface as shown in Fig. 5(b). The repulsive protuberances close to the dimer bond prevent an H motion within the same dimer row. These surface-mediated processes are roughly as probable as the ''direct'' processes shown in Fig. 4 and lead to the high value for S given in Table VI. We note that these surface-mediated processes increase the number of dangling bonds visited by the H atom. Therefore, they increase S even in the case of asymmetric dimers with less empty dangling bond sites.

Finally, this table also reveals the sticking coefficient of D to be slightly *smaller* than that of H. This is somewhat surprising since the heavier D has a larger momentum and loses more energy than H in the impact process. Indeed, at zero temperature, S of D is slightly higher than that of H. At 500 K, however, energy transfer occurs not only from the impinging atom to the lattice but also vice versa due to the lattice vibrations of the Si atoms. Since the energy transfer between D and Si is more efficient than that between H and Si, this temperature-induced energy gain is larger for the reflected D than for H. This effect reduces S of D at finite temperatures relative to H.

VI. PREDICTIONS: ELEY RIDEAL HYDROGEN ABSTRACTION FROM Si(100)2×1:H

A central question in context with hydrogen passivation of Si surfaces is how a full monolayer of H can ever be absorbed despite the efficient creation of voids in the passivation layer by H abstraction reactions such as reaction (2).[4] In this section, we study the interplay of dynamical processes that can lead to complete H passivation of Si surfaces.

First, we have calculated the equilibrium geometry of a Si(100)2×1:H surface, as depicted schematically in Fig. 8. Our model predicts a Si-Si dimer bond length of 2.43 Å (2.40 Å), an angle between the dimer bond and the Si-H bond of 112.4° (110.2°), and the angle between the dimer back bond and the Si-H bond of 112.5° (111.7°), where the first-principles LDA results[12] are given in parentheses for comparison. These results also agree well with those based on the model potential of Ref. 23.

We have used the same substrate temperature of 500 K,

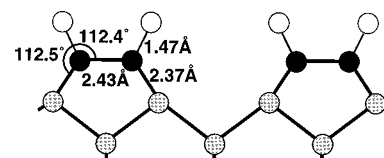

FIG. 8. Side view of the calculated equilibrium geometry of the Si monohydride surface. White circles represent H atoms, black and gray circles topmost and subsurface Si atoms.

TABLE VII. Calculated probabilities for the reactions of atomic hydrogen (H) and deuterium (D) at Si(100)2×1:D and Si(100)2×1:H surfaces, respectively. The surface temperature has been set to 500 K. As deduced from the calculated trajectories, the reactions are reflection (refl.), abstraction (abst.), adsorption (adso.), exchange (exch.), and combined processes (comb.) that consist of an exchange followed by an abstraction.

	Energy (eV)	refl.	abst.	adso.	exch.	comb.
H	0.1	0.05	0.39	0.56	0	0
	0.2	0.03	0.39	0.58	0	0
D	0.1	0.03	0.42	0.55	0	0
	0.2	0.02	0.40	0.58	0	0
	2.0	0.10	0.15	0.60	0.13	0.02

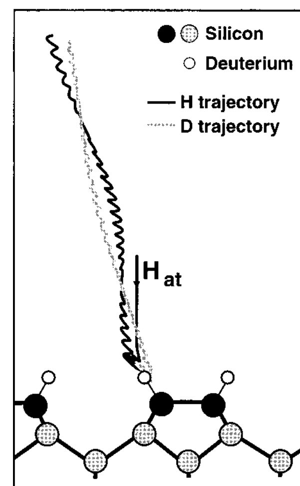

FIG. 9. Calculated H (black line) and D (gray line) trajectories for the HD-abstraction reaction, projected onto the (100),(011) plane. White circles depict the D atoms adsorbed on the surface, black and gray circles topmost and subsurface Si atoms. For clarity, the motion of the silicon atoms is not shown. Trajectories are depicted for a period of 350 fs.

same sample size, and same initial conditions for the incoming H atom as in the preceding section. Since both experiment[18] and the present theory indicate the Si(100)2×1:H surface with symmetric dimers to be the lowest energy configuration, our simulations are based on this configuration. We have also performed calculations where D has been replaced by H either on the surface or in the gas phase. For brevity, we will explicitly mention deuterium only in cases where the results differ qualitatively from those obtained with hydrogen. By computing several hundred trajectories of incoming H atoms, we have found three principal types of surface reactions, namely, (i) the approaching H gets reflected from the passivated silicon surface; (ii) the impinging H atom bonds to an H atom of the surface according to abstraction reaction (2), and an H_2 molecule leaves the surface, leaving a dangling bond behind; (iii) the H atom gets chemisorbed on the surface.

By sampling 400 trajectories for each incident energy (and isotope) we have computed the respective probabilities of these processes, as summarized in Table VII. The reflection is seen to occur with very low probability. Even for kinetic energies higher than 1.5 eV, this probability increases only slightly due to exchange processes where the impinging atom gets adsorbed at an occupied surface site while kicking out the previously adsorbed H atom. The calculated potential energy surface reveals that this exchange process can occur with no activation barrier. For low energies, however, this process is irrelevant because it is masked by the energetically more profitable Eley-Rideal abstraction that gives a potential energy gain of approximately 1.5 eV (see Sec. III E).

We now focus on the second type of surface reaction, namely the abstraction. Figure 9 shows a typical abstraction trajectory. In this example, we consider a deuterium-passivated surface and depict the projection of the three-dimensional trajectories onto the (011) and (100) plane. The motion of the Si atoms is not shown to avoid cluttering of the figure. The figure illustrates clearly that the energy gained by forming an H_2 molecule is converted into rotational and vibrational modes of the extracted HD molecule that leaves the surface in a highly excited HD molecular state. The amplitude of vibration is seen to be smaller for the heavier D than for the H atom. The abstraction and H_2 or HD formation occurs with a high probability of about 40% at low energies. Experimentally, the probability for Eley-Rideal abstraction has been estimated to lie in the range of 0.3–0.5 up to incident energies of 2.7 eV.[5] The present theory predicts a value of 0.4 for low energies, in excellent agreement with the data. For energies exceeding 1.5 eV, however, we predict a significantly reduced abstraction rate of 0.15, that has not been found in experiment.[5] This discrepancy might be caused by additional reaction paths that become relevant for high incident energies. Our analysis indicates only one additional reaction mechanism to occur at high energy, that is, a combined H exchange and subsequent abstraction. However, this process enhances the total abstraction rate only by a small amount as shown in Table VII.

Independent of the incident energy, the most likely reaction turns out to be the third type of process, that is, the adsorption of the incident H atom. It is well known that there are deep potential energy minima of the order of 2 eV for H in the second atomic layer beneath the clean Si(100) surface, in addition to the dangling bond sites.[36] In the case of a passivated H surface, there are no empty dangling bond sites but these secondary minima still persist. Our calculations confirm the existence of these adsorption sites that are depicted in Fig. 10. It shows a snapshot of the potential energy surface of an H atom moving in the (100) and (011) plane containing the dimer bond with the attached H atom. The energy minimum at -0.8 eV in the second layer reaches an absolute mininum of -1.2 eV in the plane of the second layer atom shown in gray. The fingerprints of further adsorption sites with shallow minima associated with the top Si layer can be seen in the upper left part of Fig. 10. This figure reveals another fairly deep potential minimum above the adsorbed H. However, this minimum is *not* an adsorption site but responsible for the H_2 formation that leads to the Eley-Rideal abstraction discussed above.

In conclusion, the present calculations confirm the conjecture of Ref. 4 that additionally adsorbed H atoms on hydrogenated Si surfaces act as a hydrogen reservoir that effi-

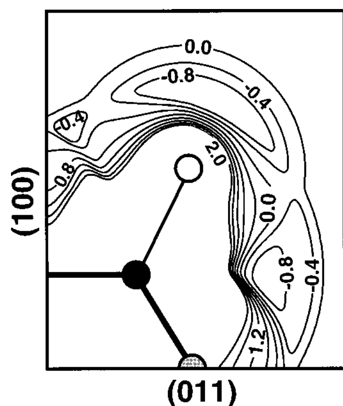

FIG. 10. Potential energy surface for an H atom near the monohydride surface. The black circle is one of the Si dimer atoms in the depicted plane. The zero of energy is taken to be the pure monohydride surface, the spacing of the contour lines is 0.4 eV. In the highly repulsive region, they are drawn up to 2.0 eV.

ciently closes the voids in the passivation layer created by the H_2 abstraction reactions.

In passing we note that this surprisingly high rate for H adsorption onto the passivated Si surface provides an *a posteriori* justification of using a symmetric dimer reconstruction for calculating the sticking coefficient on clean (100) surfaces in the preceding section. The lowest energy configuration with buckled dimers[43] is well known to lead to a strongly asymmetric electron density distribution.[30,44] If one assumes that H atoms can only be absorbed on empty dangling bond sites, S could be reduced by as much as a factor of 2 on the surface with buckled dimers (that contain one empty and one doubly occupied dangling bond) relative to the symmetric configuration with two singly occupied dangling bonds per dimer. However, it is known that the adsorption of just one H atom onto an asymmetric dimer already leads to a nearly symmetric electron distribution.[45] Since we find, in addition, that $S\approx 0.6$ for the clean as well as for the fully hydrogenated surface, it seems unlikely that S is strongly affected by the type of reconstruction that we have used.

VII. SUMMARY

In conclusion, we have developed an interatomic Si-H interaction potential that provides a basis for classical molecular-dynamics studies for a wide range of phenomena involving the interaction of hydrogen with silicon surfaces. This model potential accurately reproduces the experimentally known vibrational frequencies and bond lengths of several silicon hydrides. Furthermore, it also agrees excellently with experimental data and *ab initio* calculations for a variety of surface properties, such as diffusion barriers and paths of H at the surface and in the bulk, and for H_2 desorption activation energies.

The present model predicts a very high sticking coefficient of atomic H on clean Si (100) surfaces, $S\approx 0.6$ for incident energies in the range of a few tenths of an eV. The crucial property that determines this adsorption rate of atomic H is found to lie in the strong anisotropic shape of the dangling bond potential that acts as a guiding channel for the impinging H atom and prolongs the interaction time significantly.

We have identified three major reactions for H impinging on a fully hydrogenated surface, namely reflection, Eley-Rideal H_2 abstraction, and adsorption. The calculations predict H adsorption to be the dominant process with a probability of 60% even on an already fully passivated surface. This result explains how complete H passivation of Si surfaces can be achieved despite the efficient H_2 abstraction that generates voids in the passivation layer. It is this high adsorption rate of hydrogen that provides the source of hydrogen on the surface to close these voids.

ACKNOWLEDGMENTS

We thank Dr. P. Kratzer for providing Fig. 3 prior to publication. We also thank him, Dr. M. V. Ramana Murty, Professor J. Pollmann, Dr. P. Krüger, and Professor W. Brenig for many helpful discussions, and Dr. A. Spitzer and Dr. A. Kersch for valuable guidance throughout the project. We gratefully acknowledge financial support by Siemens AG.

[1] A. C. Levi and M. Kotrla, J. Phys.: Condens. Matter **9**, 299 (1997).
[2] C. Isobe, H. C. Cho, and J. E. Crowell, Surf. Sci. **295**, 99 (1993).
[3] Y. Wang, M. J. Bronikowski, and R. J. Hamers, Surf. Sci. **311**, 64 (1992).
[4] D. D. Koleske and S. M. Gates, J. Chem. Phys. **101**, 3301 (1994).
[5] S. A. Buntin, J. Chem. Phys. **105**, 2066 (1996).
[6] U. Höfer, Appl. Phys. A: Mater. Sci. Process. **63**, 533 (1996).
[7] W. Widdra, S. Yi, and W. Weinberg, Phys. Rev. Lett. **74**, 2074 (1995).
[8] M. Copel and R. M. Tromp, Phys. Rev. Lett. **72**, 1236 (1994).
[9] P. Nachtigall, K. D. Jordan, and C. Sosa, J. Chem. Phys. **101**, 8073 (1994).
[10] A. Gross, M. Bockstedte, and M. Scheffler, Phys. Rev. Lett. **79**, 701 (1997).
[11] A. Silva, M. Radeke, E. Carter, and M. G. Sherman, Surf. Sci. Lett. **381**, L628 (1997).
[12] J. E. Northrup, Phys. Rev. B **44**, 1419 (1991).
[13] P. Nachtigall and K. D. Jordan, J. Chem. Phys. **102**, 8249 (1995).
[14] E. Pehlke and M. Scheffler, Phys. Rev. Lett. **74**, 952 (1995).
[15] A. P. Smith, J. K. Wiggs, and H. Jonsson, J. Chem. Phys. **102**, 1044 (1995).
[16] P. Bratu, K. L. Kompa, and U. Höfer, Chem. Phys. Lett. **251**, 1 (1996).
[17] D. D. Koleske and S. M. Gates, J. Chem. Phys. **99**, 5619 (1993).
[18] J. Boland, Surf. Sci. **261**, 17 (1992).
[19] K. Oura, J. Yamane, K. Umezawa, M. Naitoh, and T. Hanawa, Phys. Rev. B **41**, 1200 (1990).
[20] P. M. Agrawal, D. L. Thompson, and L. M. Raff, J. Chem. Phys. **88**, 5984 (1988).

[21] I. Kwon and R. Biswas, Phys. Rev. B **45**, 3332 (1988).
[22] M. V. Ramana Murty and H. Atwater, in *Mechanisms of Thin Film Evolution*, edited by S. M. Yalisore, C. V. Thompson, and D. J. Eaglesham, MRS Symposia Proceedings No. 317 (Materials Research Society, Pittsburgh, 1994), p. 355.
[23] M. V. Ramana Murty and H. Atwater, Phys. Rev. B **51**, 4889 (1995).
[24] J. Tersoff, Phys. Rev. B **38**, 9902 (1988).
[25] D. W. Brenner, Phys. Rev. B **42**, 9458 (1990).
[26] H. Balamane and T. Halicioglu, Phys. Rev. B **46**, 2250 (1992).
[27] D. W. Brenner, Mater. Res. Bull. **21**, No. 2, 36 (1996).
[28] D. E. Milligan and M. E. Jacox, J. Chem. Phys. **52**, 2594 (1970).
[29] J. Dabrowski and M. Scheffler, Appl. Surf. Sci. **56**, 15 (1992).
[30] P. Krueger and J. Pollmann, Phys. Rev. Lett. **74**, 1155 (1995).
[31] A. Ramstadt and G. Brooks, Phys. Rev. B **51**, 14 504 (1995).
[32] C. Van de Walle, Phys. Rev. B **49**, 4579 (1994).
[33] S. Estreicher, Mater. Sci. Eng., R. **14**, 319 (1995).
[34] S. Estreicher, Phys. Rev. B **36**, 9122 (1987).
[35] M. R. Radeke and E. A. Carter, Phys. Rev. B **54**, 11 803 (1996).
[36] A. Vittadini, A. Selloni, and M. Casarin, Surf. Sci. Lett. **289**, 625 (1993).
[37] C. J. Wu and E. A. Carter, Phys. Rev. B **46**, 4651 (1992).
[38] G. Brocks, P. J. Kelly, and R. Car, Phys. Rev. Lett. **66**, 1729 (1991).
[39] P. Kratzer (unpublished).
[40] D. C. Rapaport, *The Art of Molecular Dynamics Simulation* (Cambridge University Press, Cambridge, 1995).
[41] J. T. Law, J. Chem. Phys. **30**, 1568 (1959).
[42] U. Bischler, P. Sandl, E. Bertel, T. Brunner, and W. Brenig, Phys. Rev. Lett. **70**, 3603 (1993).
[43] P. Krueger and J. Pollmann, Phys. Rev. B **52**, 13 753 (1995).
[44] H. M. Tütüncü, S. J. Jenkins, and G. P. Srivastava, Phys. Rev. B **56**, 4656 (1997).
[45] A. Vittadini, A. Selloni, and M. Casarin, Phys. Rev. B **49**, 11 191 (1994).